

# Validation of Occupant Trajectory Model using the Ford Expedition Dolly Rollover Experimental Test Data

2013-01-0472

Published  
04/08/2013

Chad Hovey  
Hovey Consulting LLC

Elizabeth Raphael and Henry Xu  
Delta V Biomechanics Inc.

Copyright © 2013 SAE International  
doi:[10.4271/2013-01-0472](https://doi.org/10.4271/2013-01-0472)

## **ABSTRACT**

In 2008, Hovey *et al.* [1] published a mathematical analysis that, for the first time, incorporated yaw data into the trajectory analysis, yielding occupant ejection results that are three-dimensional. We extend on that work to investigate the ability of the mathematical model to predict outcomes of the Ford Expedition dolly rollover test, details of which have been published in Carter *et al.* [2], Exponent [3], and Luepke *et al.* [4]. This research validates our occupant trajectory model with the Expedition dolly rollover experimental test data.

Previous research had modeled the Expedition rollover test as a two-dimensional, straight-line, roll-only configuration, assuming yaw effects were negligible [17]. We incorporated the longitudinal and lateral components of the vehicle trajectory, eliminating the straight-line limitation. Moreover, we included yaw in addition to roll. Both enhancements resulted in a higher fidelity occupant ejection description. Novel to this work is the inclusion of experimental data from the dolly rollover test performed by Exponent [3] and analyzed by Carter *et al.* [2] to validate the model developed by Hovey *et al.* [1].

Also novel to this work is the application of case-specific vehicle speed and roll rate data from the Expedition dolly rollover test. Previous efforts with a two-dimensional ejection analysis have modeled rollover events with the same roll rate function [17], thereby homogenizing the underlying uniqueness of a particular accident. Every rollover accident has a distinct signature, embodied in its translational and

rotational degrees of freedom. We capture this uniqueness with case-specific, experimental data.

The results of this effort indicate our model [1] predicts experimentally obtained test results. This validation provides analysts further confidence in the use of the previously developed model.

## **INTRODUCTION**

Vehicle dynamics of rollover events, in the absence of occupant descriptions, has been well researched [2, 5, 6, 7, 8, 9, 10]. Occupant kinematics in rollovers, without consideration of ejections, has also been examined [11-12, 22, 23, 24, 25].

Occupant trajectories in the context of pedestrian-vehicle impacts and motorcycle accidents have been considered [13, 14, 15, 16]. These models, given a known total distance from launch to point of rest (POR), describe an occupant's airborne trajectory and ground sliding distance.

In the context of rollover accidents, the ejection velocity can be calculated as a function of vehicle and occupant kinematics, however, the time and vehicle location when the occupant is ejected is unknown. It is useful to predict these unknown data, which has an impact on the injury biomechanics, such as how far the occupant was thrown from the vehicle, or if there was post-ejection vehicle-ejectee contact.

Use of a generic roll rate function is common. Funk and Luepke [17] proposed a generalized vehicle dynamics model, employing a roll rate function as a combination of a linear function and a square root function, zero at the initial and final time points, and peaking early in the time evolution.

Herrera and Najera [18] used a trapezoidal roll rate function, which starts at zero, ascends linearly to a peak roll rate, plateaus at a constant value, then descends linearly to zero. As with the approaches in [1] and [17], Herrera's roll rate function, when integrated over time, equals the number of rolls in the rollover event, as expected and required for mathematical consistency.

Rose and Beauchamp [9] proposed replacing the constant translational deceleration assumption with a vehicle-to-ground impact model that allowed the vehicle's deceleration to vary throughout the rollover event. Changes in linear velocity were related to changes in angular velocity, which provided roll rate versus time curves that followed experimental results.

The simplicity in which an ejection solution can be constructed is a clear advantage of pre-formulated roll rate functions. The disadvantage is that this approach eliminates the uniqueness of a particular rollover event, and does not model roll rate time evolutions differently from the *a priori* assumed form. Our approach proposes the use of data tailored to a specific accident.

McCarron [19] used our model [1] for occupant dynamics. He showed occupant point of rest data on the accident reconstruction plan view diagrams, parameterized by time. The result appeared as a “spray pattern.” A mathematically feasible ejection solution occurred when the spray contour intercepted the known occupant point of rest.

Funk *et al.* [20] used their two-dimensional model to investigate ATD ejections in a rollover test of a 2004 Volvo XC90, and two human ejections from rollover traffic accidents captured on video tape. In all cases, Funk reported model inputs were optimized, which amounted to parameterizing and tuning free variables so that the calculations matched observed results. For cases where the answer is unknown beforehand (*e.g.*, a predictive scenario, not a retrospective study), we have advocated using a range of occupant-to-ground friction values, as detailed in [1].

## METHODS

We adopt our previously developed model [1], but with two modifications. First, we set radial velocity components  $\dot{r} = 0$  for all time, to facilitate meaningful comparisons to the two-

dimension model results of [17]. Second, we make our notation for reference frames more compact.

## Reference Frames

[Figure 1](#) illustrates the reference frames. Let the inertial reference frame  $\mathcal{F}$  have unit vectors  $[\hat{\mathbf{f}}_1, \hat{\mathbf{f}}_2, \hat{\mathbf{f}}_3]$  at origin point  $F$ . Unit vector  $\hat{\mathbf{f}}_1$  points to the right of the page. Unit vector  $\hat{\mathbf{f}}_2$  points the top of the page. Unit vector  $\hat{\mathbf{f}}_3$  points out of the page, and is perpendicular to a level plane of vehicle travel. These unit vectors correspond to the easting, northing, and elevation vectors in a plan view survey coordinate system, respectively. All unit vectors used in this paper are dextral, orthonormal, ordered triads. Note that our coordinate system uses the  $z$  direction as up. This is different from the SAE convention, which uses the  $z$  direction as down.<sup>1</sup>

Let the carrier frame  $\mathcal{A}$  be attached to the vehicle's center of mass at point  $V$ . The carrier frame has unit vectors  $[\hat{\mathbf{a}}_1, \hat{\mathbf{a}}_2, \hat{\mathbf{a}}_3]$ . Unit vector  $\hat{\mathbf{a}}_1$  points toward the front of the vehicle. Unit vector  $\hat{\mathbf{a}}_2$  points to the left of the vehicle, with the vehicle in a nonrolling configuration. Unit vector  $\hat{\mathbf{a}}_3$  points to the roof of the vehicle, with the vehicle in a non-rolling configuration. The carrier frame translates with the vehicle frame, but is not attached to the vehicle. Therefore, the carrier frame does not rotate with roll  $\theta$  of the vehicle with respect to the vehicle's roll axis the  $\hat{\mathbf{b}}_1$  (equivalently  $\hat{\mathbf{a}}_1$ ). The carrier frame rotates with the yaw  $\psi$  of the vehicle with respect to the inertial frame along the vertical axis  $\hat{\mathbf{f}}_3$  (equivalently  $\hat{\mathbf{a}}_3$ ).

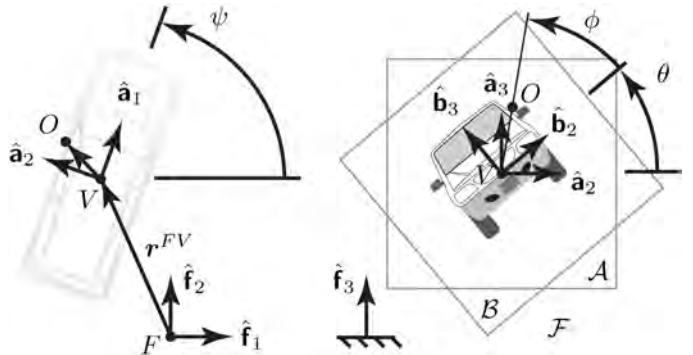


**Figure 1. Illustration of state variables, points, bases, and inertial  $\mathcal{F}$ , carrier  $\mathcal{A}$ , and vehicle  $\mathcal{B}$  reference frames in a top view (left subfigure) and vehicle front view (right subfigure).**

Let the vehicle frame  $\mathcal{B}$  be fixed to the vehicle's center of mass at point  $V$ . The vehicle frame has unit vectors  $[\hat{\mathbf{b}}_1, \hat{\mathbf{b}}_2, \hat{\mathbf{b}}_3]$ . Unit vector  $\hat{\mathbf{b}}_1$  points to the front of the vehicle. Unit

<sup>1</sup>We choose the  $z$  axis as up because we are primarily concerned with the ejected occupant's motion, which naturally lends itself to positive values indicating the occupant's elevation above ground level.

**Table 1.** Case-specific vehicle state variables at discrete times throughout the Expedition dolly rollover event.

point (#)	$t$ (sec)	$x$ (feet)	$y$ (feet)	$\psi$ (deg)	$\theta$ (deg)	$\dot{x}$ (mph)	$\dot{y}$ (mph)	$\dot{\psi}$ (deg/s)	$\dot{\theta}$ (deg/s)
1	0	-122.5	10.8	-90	-45	43.2	0	0	0
2	0.408	-98.0	10.75	-90	-89.9	36.6	-0.139	-0.01	-292
3	0.584	-89.1	10.7	-90	-173.4	32.5	-0.182	-0.02	-522
4	0.784	-80.1	10.65	-90.01	-287.4	29.0	-0.200	-0.03	-577
5	0.932	-74.0	10.6	-90.01	-373.9	28.2	-0.313	-0.06	-555
6	1.104	-66.9	10.5	-90.03	-464.2	27.8	-0.569	-0.11	-513
7	1.288	-59.7	10.3	-90.05	-556.2	25.1	-0.882	-0.24	-488
8	1.488	-52.9	10.0	-90.12	-651.2	21.1	-1.13	-0.54	-460
9	1.708	-46.5	9.6	-90.29	-749.1	19.3	-1.49	-1.99	-430
10	2.176	-34.3	8.4	-91.79	-943.4	15.8	-2.06	-11.81	-385
11	2.752	-22.6	6.4	-103.5	-1148	12.5	-2.79	-30.36	-312
12	3.516	-9.1	2.8	-134.4	-1354	11.4	-3.61	-25.12	-225
13	3.992	-2.3	0	-139.1	-1440	7.5	-6.17	-6.29	-177
14	4.164	-0.7	-2.1	-139.5	-1470	5.1	-3.31	-1.61	-69.4
15	5.008	0	0	-140	-1440	0	0	0	0

vector  $\hat{\mathbf{b}}_2$  points to the left of the vehicle. Unit vector  $\hat{\mathbf{b}}_3$  points to the roof of the vehicle.

## Vehicle Evolution

To obtain vehicle speed data,  $\mathcal{F}v^V$  and  $\mathcal{F}\omega^B$ , we utilize data and the accident reconstruction diagram in [2] to approximate position and orientation time history. To obtain time derivative data, we construct midpoint values as

$$\dot{x}_{n-\frac{1}{2}} = \frac{x_n - x_{n-1}}{t_n - t_{n-1}}, \quad \dot{x}_{n+\frac{1}{2}} = \frac{x_{n+1} - x_n}{t_{n+1} - t_n}, \quad (1)$$

for the  $x$  degree of freedom. All other degrees of freedom time derivatives are calculated in an analogous manner. Then, at any specific time  $t_n$ , the value of the time derivative is calculated as

$$\dot{x}_n = \frac{1}{2} \left( \dot{x}_{n-\frac{1}{2}} + \dot{x}_{n+\frac{1}{2}} \right). \quad (2)$$

This approach produces the Expedition dolly rollover specific state variables at discrete times throughout the rollover event, recorded in Table 1. Initial and final conditions with known quiescent values are set to zero directly.

Figure 2 shows continuous vehicle time evolution data, obtained from piecewise linear interpolation of the discrete data, taken at 15 discrete vehicle templates in [2].<sup>2</sup> Vehicle

roll and longitudinal position are obtained by integrated roll rate and downstream speed over time. Figure 2 also shows experimental data, produced in [2], for vehicle downstream speed and roll rate.

## Occupant at Ejection

In our previous work [1], we described the position vector of the occupant at ejection  $\mathbf{r}^{FO} \in \mathbb{R}^3$  as the vector sum of  $r^{FV}$  and  $r^{VO}$ , written explicitly as

$$\mathbf{r}^{FO} = x \hat{\mathbf{f}}_1 + y \hat{\mathbf{f}}_2 + z \hat{\mathbf{f}}_3 + \chi \hat{\mathbf{b}}_1 + \rho \cos \phi \hat{\mathbf{b}}_2 + \rho \sin \phi \hat{\mathbf{b}}_3. \quad (3)$$

For meaningful comparisons with the 2D model of [17], we select the same initial position, as shown in Figure 3, for the occupants at ejection:

- 1L ( $\rho = 52$  inches = 1.32 m,  $\phi = 50^\circ$ ),
- 1R ( $\rho = 48$  inches = 1.22 m,  $\phi = 145^\circ$ ), and
- 2R ( $\rho = 48$  inches = 1.22 m,  $\phi = 145^\circ$ ).

Occupant seating position within the vehicle is denoted with a front-to-back, left-to-right nomenclature. The United States driver position holds the first row left-side occupant, and is abbreviated as “1L.” Other occupants follow this pattern, row number followed by L or R for left or right of the vehicle, respectively.

<sup>2</sup>Note that Carter [2], in Appendix B, Test 1, Vehicle Position Layout, uses an initial time of 0.140 s for template “0,” for which we adjust our clock to start at 0.00 s for the same template. As expected, Carter’s final time stamp of 5.148 s corresponds to our 5.008 s.

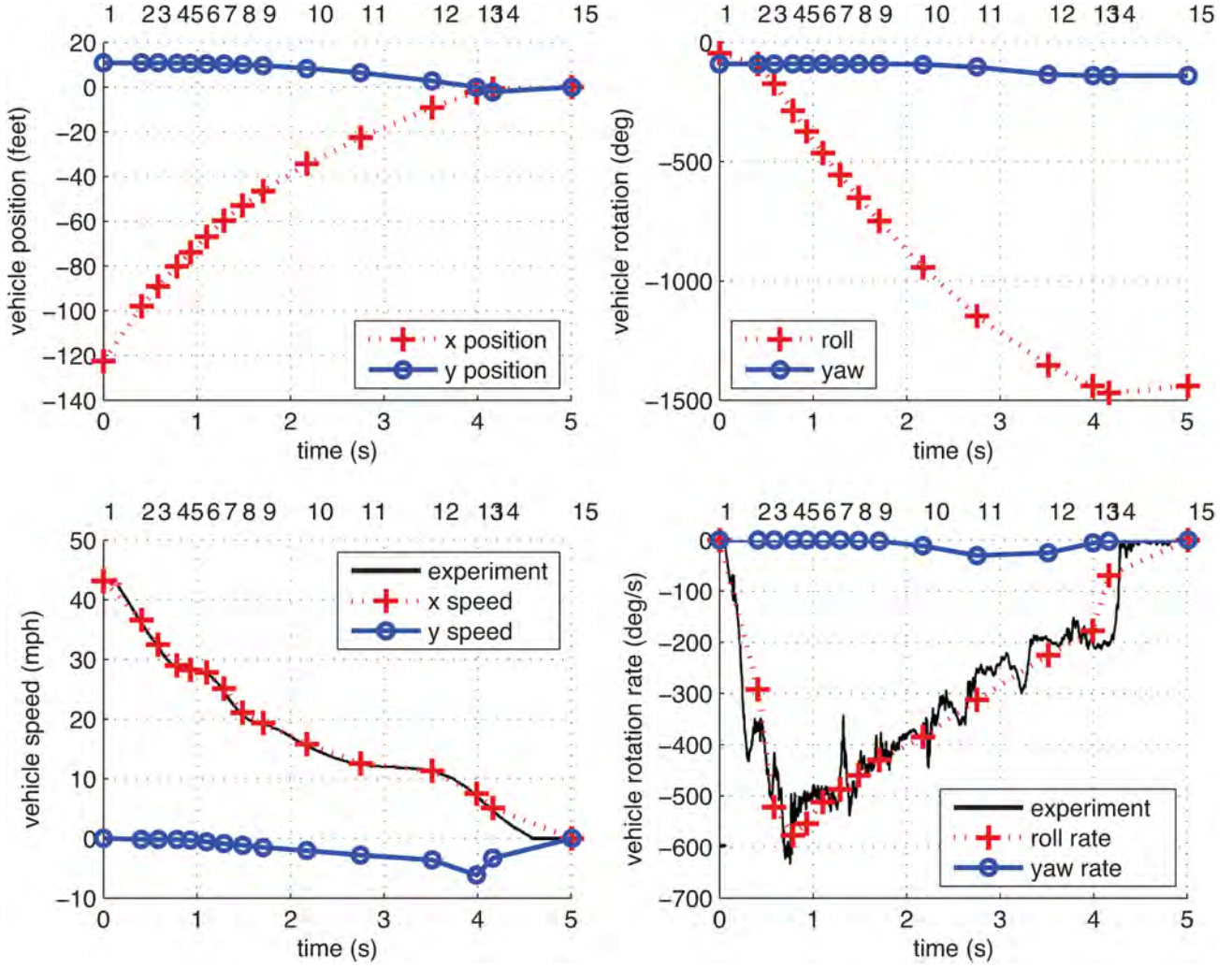


**Figure 2.** Vehicle state data as a function of time, with discrete points 1...15 indicated, and experimental data for vehicle translational and rotational speeds shown.

Since there is no fore-aft component of the initial position in the 2D model, our selection of  $\chi_{1L} = \chi_{1R} = 0$  inches (0 m) in our 3D model will, as a special case, correspond to the 2D model positions. We select  $\chi_{2R} = -30$  inches (0.76 m) for the second row right occupant, as shown in Figure 4.

We use ground sliding coefficient of friction for 1L, 1R, and 2R as 0.56, 0.67, and 0.73, respectively, which comport with previously published values [14,15,16, 21]. Although we utilize discrete friction values in this paper for the purposes of comparison with results published in [17], our normal practice is to parameterize the ground friction effects, which results in an upper and lower bound for occupant position of rest.

We consider only the 1L, 1R, and 2R occupants because they, after ejection, avoid contact with the vehicle. Our model illustrates the simultaneous time evolution of the ejected occupant and the vehicle. Therefore, our model is capable of showing vehicle overrun of the occupant after ejection.

Currently, however, we have not implemented a vehicle-to-ejectee contact formulation. Therefore, the analyses with the 3L and 3R occupants are not included in the cases presented here. The 2L occupant was not ejected in the test.

We described the velocity of an occupant  $\mathcal{F}\mathbf{v}^O \in \mathbb{R}^3$  ejected from a rollover vehicle with non-trivial yaw effects as

$$\mathcal{F}\mathbf{v}^O = \mathcal{F}\mathbf{v}^V + \mathcal{B}\mathbf{v}^O + \mathcal{F}\boldsymbol{\omega}^B \times \mathbf{r}^{VO}, \quad (4)$$

where  $\mathcal{F}\mathbf{v}^V$  is the velocity of the vehicle relative to the inertial frame,  $\mathcal{B}\mathbf{v}^O$  is the velocity of the occupant relative to the vehicle frame,  $\mathcal{F}\boldsymbol{\omega}^B$  is the angular velocity of the vehicle in the inertial frame, and  $\mathbf{r}^{VO}$  is the position vector from the vehicle at point  $V$  to the occupant at point  $O$ . The explicit form of  $\mathcal{F}\mathbf{v}^O$  written in the  $[\hat{\mathbf{f}}_1, \hat{\mathbf{f}}_2, \hat{\mathbf{f}}_3]$  basis is quite long, and can be found in the Appendix. All results presented here, including data in Table 3, use  $\mathcal{B}\mathbf{v}^O = 0$  in Eq. (4).

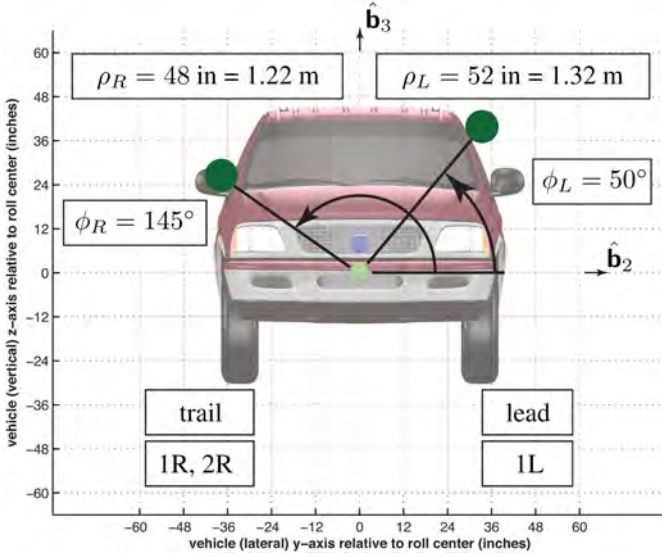


**Figure 3.** Vehicle front view showing initial positions of the occupants at ejection.

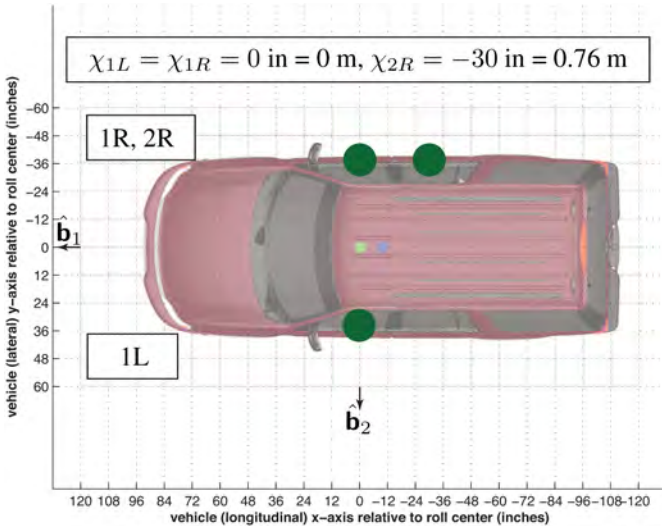


**Figure 4.** Vehicle top view showing initial positions of the occupants at ejection.

## Occupant at Point of Rest (POR)

Our model predicts multiple occupant ejection possibilities, from the beginning to the end of the rollover. A possible ejection solution is chosen if its predicted position of rest matches the known ejectee position of rest.

In the engineering practice of ejection analysis, real world occupant data often only includes the ejectee's point of rest; it does not offer any ejection data such as point of ejection, ejection speed, or ejection height, for example. Therefore, the analyst must conceptually start with the final conditions of the accident, then work backwards in time. We adopt this same methodology for study of the Expedition dolly rollover test, using point of rest data for the ATDs, recorded in Table

2, as known. The experimental POR data is then compared with calculated POR data to assess the ability of the model to predict occupant ejections.

**Table 2.** Experimental ATD point of rest (POR) observed in the Expedition dolly rollover test performed by Exponent [3] and analyzed by Carter et al. [2] and Luepke et al. [4].

Vehicle POR to ATD POR	symbol	ATD Seat Position		
		1L	1R	2R
$x$ (feet)	$\hat{\mathbf{f}}_1 \cdot \mathbf{r}_{\text{rest}}^{VO^*}$	89.8	40.5	42.7
$y$ (feet)	$\hat{\mathbf{f}}_2 \cdot \mathbf{r}_{\text{rest}}^{VO^*}$	7.16	3.87	7.87
$\sqrt{x^2 + y^2}$ (feet)	$\  \mathbf{r}_{\text{rest}}^{VO^*} \ $	90.1	40.7	43.4

## RESULTS

Vehicle and occupant evolution data are presented numerically in Table 3 and graphically in Figure 5. Results from our model, labeled as “3D,” are compared with data recorded in [17], labeled as “2D.” Where applicable, results from these two models are compared. A dash (“-”) is shown when data for the 2D model was either not reported (*e.g.*, ejection and landing times); or, not applicable (*e.g.*, yaw angle and rate at ejection). Results are ordered by occupant label reference, not by occupant ejection time.

We note point  $O$  as the position of the occupant as predicted by the model. In contrast, we denote point  $O^*$  as the actual position of the occupant, known from experimental data.

We define an error measure of predicted versus actual occupant point of rest as

$$\epsilon_{\text{rest}}^{OO^*} = \frac{\| \mathbf{r}_{\text{rest}}^{OO^*} \|}{(\Delta s_{\text{air}}^O + \Delta s_{\text{slide}}^O)}. \quad (5)$$

The predicted occupant trajectory positions from ejection to rest matched actual data well, with an average error rate of approximately 4%, range [0.98%, 6.3%].

Figure 5 illustrates plan and side views of the vehicle position and orientation at time of occupant ejection, as recorded in Table 3. The ejection time, to two significant figures, is recorded as the left-most green dot, with motion evolving left-to-right. Subsequent times for occupant air travel are recorded at 200 ms intervals. The position of first ground impact is shown with the left-most purple dot, at the time nearest the next 200 ms interval. The position of occupant rest is shown with a red dot, and indicated with the final time stamp. Notice the point of rest is attained first for the 1R occupant (4.4 s), followed by the 2R occupant (4.6 s), the vehicle ( $\approx 5$  s), and the 1L occupant (5.4 s), as confirmed by downstream video footage of the dolly rollover test [3].

**Table 3. Vehicle and occupant details at each ejection solution-vehicle roll angle, vehicle distance from trip, vehicle speed, occupant ejection angle, occupant ejection speed, occupant vertical landing speed, occupant maximum height, occupant horizontal distance in the air, occupant horizontal distance on the ground, and combined air and ground distance. The 2D indicates Funk et al. [17] data. The 3D indicates use of the Hovey et al. [1] model with Expedition dolly rollover data described here in Table 1 and Figure 2.**

Description	symbol	ATD Seat Position						units
		1L		1R		2R		
		3D	2D	3D	2D	3D	2D	
ATD ejection time	$t_{\text{eject}}^O$	1.48	-	0.86	-	1.65	-	seconds
Vehicle distance from trip at ejection	$\Delta s_{\text{eject}}^V$	74.7	50	51.9	26	79.5	55	feet
Vehicle speed at ejection	$\ \mathcal{F}\mathbf{v}_{\text{eject}}^V\ $	19.9	22	29.1	28	18.5	20	mph
Vehicle roll number at ejection	$\theta_{\text{eject}}^V$	1.80	1.76	0.92	0.91	2.01	1.98	revolutions
Vehicle roll rate at ejection	$\dot{\theta}_{\text{eject}}^V$	461	467	566	525–615	438	440	deg/sec
Vehicle yaw angle at ejection	$\psi_{\text{eject}}^V$	-90.1	-	-90.0	-	-90.2	-	degrees
Vehicle yaw rate at ejection	$\dot{\psi}_{\text{eject}}^V$	-0.53	-	-0.04	-	-1.61	-	deg/sec
ATD ejection angle	$\beta_{\text{eject}}^O$	17.2	19	40.1	45	25.9	27	degrees
ATD ejection speed	$\ \mathcal{F}\mathbf{v}_{\text{eject}}^O\ $	43.2	45	41.5	41	35.9	36	mph
ATD air time	$\Delta t_{\text{air}}^O$	1.46	1.62	2.53	2.71	1.64	1.66	seconds
ATD air distance	$\Delta s_{\text{air}}^O$	88.4	100	118	117	77.6	77	feet
ATD maximum trajectory height	$h_{\text{max}}^O$	12.4	14	27.6	31	13.8	14	feet
ATD landing time	$t_{\text{land}}^O$	2.94	-	3.39	-	3.29	-	seconds
ATD vertical landing speed	$\mathcal{F}\mathbf{v}_{z,\text{land}}^O$	-19.3	-20.6	-28.7	-30.2	-20.4	-17.3	mph
ATD slide distance	$\Delta s_{\text{slide}}^O$	50.6	44	9.31	4	17.3	13	feet
ATD (air + slide) distance	$\Delta s_{(\text{air+slide})}^O$	139	144	127	121	94.9	90	feet
Vehicle POR to ATD predicted POR $x$	$\hat{\mathbf{f}}_1 \cdot \mathbf{r}_{\text{rest}}^{VO}$	83.5	85	46.1	37	43.6	36	feet
Vehicle POR to ATD predicted POR $y$	$\hat{\mathbf{f}}_2 \cdot \mathbf{r}_{\text{rest}}^{VO}$	6.15	-	9.59	-	8.12	-	feet
Vehicle POR to ATD predicted distance	$\ \mathbf{r}_{\text{rest}}^{VO}\ $	83.7	-	47.1	-	44.3	-	feet
ATD POR distance predicted from actual	$\ \mathbf{r}_{\text{rest}}^{OO^*}\ $	6.4	-	8.0	-	0.93	-	feet
ATD POR error	$\epsilon_{\text{rest}}^{OO^*}$	4.6	-	6.3	-	0.98	-	percent

Vehicle trip and rest, occupant ejection, and occupant rest are included, adapted from [2, 4]. Actual occupant PORs are indicated with red circles with a radius of 5 feet (1.52 m).

At predicted ejection times, vehicle and occupant visualization are extracted from film analysis [3], and shown in Figure 6. Approximate occupant ejection positions, vehicle roll positions, and vehicle roll rate, shown graphically in Figure 5, coincide with tabular data in Table 3.

## DISCUSSION

The motion of occupants ejected from rollover vehicles with yaw can be reliably predicted by our ejection model. Here we have demonstrated if vehicle accident reconstruction input data is of a high quality, the resulting predictions for how an occupant is ejected is also of high quality. Several authors have published research devoted to accurately reconstructing the vehicle's rollover dynamics [2, 5,6,7,8,9, 18, 20]. If the

general principles embodied in the aforementioned reconstruction publications are followed, this validation shows that the analyst can expect to obtain a reliable prediction of occupant ejection using the model examined here and originally developed in [1].

In this specific case, the accuracy of the model to predict longitudinal occupant point of rest largely depends on the vehicle's downstream translational speed, the vehicle's roll rate, the vehicle's orientation, and the occupant-to-ground friction. Here, the most significant contribution from the vehicle's translational speed occurs at the beginning of the roll event, where the vehicle trips at 43.2 mph (69.5 kph).

After the trip, the vehicle quickly achieves its peak roll rate, as translational kinetic energy is transformed to rotational kinetic energy. This transformation is observed by comparing the relatively large decrease in translational speed during the

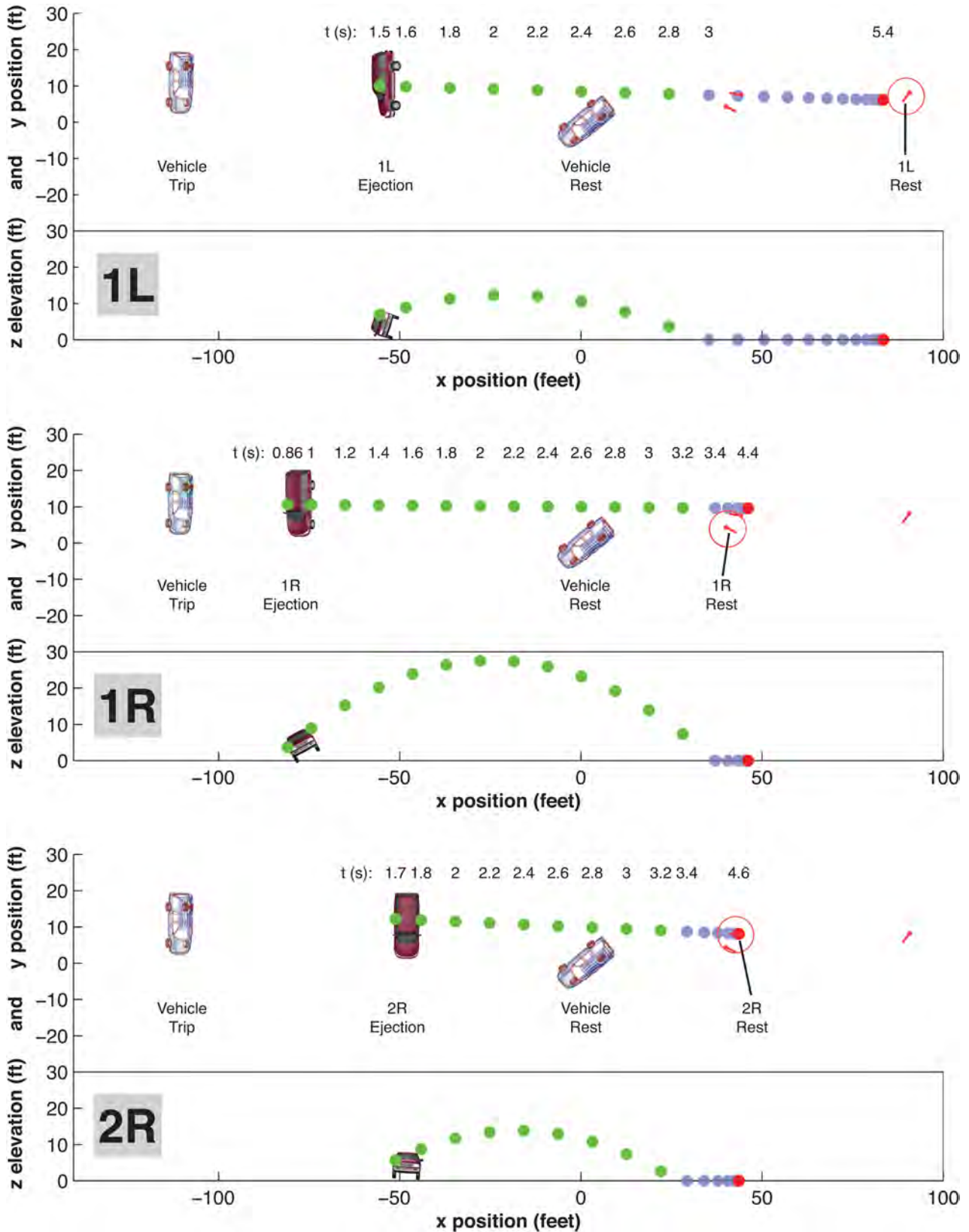


Figure 5. Accident reconstruction diagram in plan view adapted from [2], showing vehicle positions at trip, at occupant ejection and at rest; predicted occupant ejection and trajectory at 200 ms intervals in the air (green), on the ground (purple) and at rest (red); experimental ATD point of rest (red circle).



Figure 6. Images from Exponent's high speed video [3] of cameras, onboard and off board, front and rear, showing ejections of the 1L, 1R, and 2R ATDs.

first 1000 milliseconds of the rollover event to the relatively large increase in rotational speed during the same time interval, as shown in Figure 2.

The peak roll rate drives the occupant ejection speed when the roll rate is maximum. Consider a peak roll rate of 600 degrees per second and an occupant ejection radius of 4 feet (1.21 m), a condition that exists in this dolly rollover experiment just before the first 1000 milliseconds has elapsed. Under these conditions, the roll rate creates a tangential speed of approximately 29 mph (47 kph), nearly the same as the vehicle's downstream speed at that same moment.

Roll angle is also an important parameter. Depending on the orientation of the vehicle, the tangential speed can serve to either amplify or diminish the occupant's total ejection speed, which is a vector sum of all the speeds arising from vehicle translation and rotation.

The relative velocity of the occupant with respect to the vehicle frame,  $\mathcal{B}v^O$  in Eq. (4), will have an effect on the total occupant ejection velocity. We purposefully set this relative velocity term to zero so that meaningful comparisons to Funk *et al.* [17] could be made. Nonetheless, the analyst can readily understand nonzero relative velocity effects:

- For the sake of illustration, consider time point 4 ( $t = 0.784$  s) in [Table 1](#) and use a 4 feet radius for the occupant at ejection. At this time, the contribution to the ejection speed from the vehicle's translation is 29.0 mph. The contribution to the ejection speed for the vehicle's roll rate of 577 degrees per second is 27.5 mph.

- If these two vectors are aligned, the occupant is at the 12 o'clock position (relative to the carrier frame  $\mathcal{A}$ ) and the resulting speed is 56.5 mph downstream. A non-zero radial velocity vector would point skyward, amplifying the trajectory.

- If these two vectors are in opposite directions, the occupant is at the 6 o'clock position and the resulting speed is 1.5 mph downstream. A non-zero radial velocity vector would point downward, having no effect on the occupant's trajectory since the ground blocks the portal.

- In general, the relative radial velocity causes a contribution to the occupant's ejection velocity directed outward from the center of vehicle rotation to the perimeter of the vehicle.

In practice, we often use quiescent relative speeds as a starting point, setting both  $\dot{\rho} = 0$  and  $\dot{\chi} = 0$ , in [Eq. \(9\)](#) and [Eq. \(8\)](#), respectively. Then, we do a parameter sweep, bounding our relative velocity term  $\dot{\rho}$  above by calculating a maximum radial speed in [Eq. \(9\)](#) from the maximum centripetal acceleration created by the vehicle's roll rate, as described in detail in [1]. For rollovers, we typically use  $\dot{\chi} = 0$  unless there is something unique to the particular accident to indicate differently. In our experience, use of the bounded approach described above leads the analyst to the same general ejection solution candidates.

For planar yaw accidents (without rolling), non-trivial relative velocity is useful to characterize the occupant's ejection speed with respect to the vehicle's carrier speed, which changes abruptly before and after a side impact, for example.

Generally, for both roll and yaw cases, should the analyst deem the occupant relative velocity (generically  $\dot{s}$ ) to be of interest, it may be estimated by determining the  $g$  field experienced by the occupant, integrating with respect to time over some crash or time interval interest, approximating a relative speed  $\dot{s}_t = gt + \dot{s}_0$ , and apportioning  $\dot{s}_t$  between  $\dot{\rho}$  and  $\dot{\chi}$  as dictated by the geometry of the problem. A concrete and slightly more elaborate example of this approach was detailed in our previous paper [1].

A full sensitivity analysis of the relative velocity term, as well as all other terms contributing to the ejection velocity would be a fruitful area of future study. Sensitivity analysis of occupant-to-ground sliding friction would also be interesting. Finally, a film study of the Expedition dolly rollover test to ascertain relative ejection speeds would be

valuable. Sensitivity and relative speed estimates are beyond the scope of this paper, and therefore are a limitation of the present study.

The predicted 1L occupant longitudinal point of rest was just short of the 5 feet (1.52 m) radius target drawn around the ATD's actual point of rest. The friction value used for the 1L occupant was 0.56, the lowest value of all three cases. The results indicate that a lower value could be justified, allowing the occupant to undergo a larger sliding distance. By contrast, the predicted 1R occupant longitudinal point of rest was just past the target point, indicating a value of greater than 0.67 could be justified. Finally, the predicted 2R occupant longitudinal point of rest was well predicted.

The results for occupant sliding predictions underscore the importance of using a range of friction values, a practice advocated in our previous work [1]. Differences in predicted versus actual points of rest can result from a number of different sources, including occupant relative motion within the vehicle, occupant frictional characteristics with the ground, and vehicle roll rate, roll angle, yaw rate, yaw angle, velocity, and position. Precision in vehicle dynamics data improves occupant kinematics predictions.

In contrast to longitudinal point of rest, the latitudinal point of rest is driven largely by vehicle yaw and yaw rate. In the Expedition experiment, all ATDs were ejected by 1.65 seconds. During this same time interval, the yaw rate was less than 2 degrees per second, indicating yaw angle had a more profound effect than yaw rate on the occupant's latitudinal point of rest. The 1L and 2R occupant latitudinal points of rest were well predicted by the model. The predicted 1R occupant latitudinal point of rest was about 5 feet (1.52 m) to the left of the experimental point of rest.

This result illustrates the sensitivity of occupant latitudinal point of rest to vehicle yaw angle. Consider the 1R case: An approximate 5 feet (1.52 m) left-of-center deviation occurred over a total occupant throw and slide distance of approximately 127 feet (38.7 m), which arose from vehicle yaw deviations of between 2 and 3 degrees. Vehicle yaw deviations result from error ranges inherent in every accident reconstruction. For example in our case, the Expedition's yaw can be expected to deviate from the calculated yaw of the reconstruction by 2 to 3 degrees. Indeed, if the vehicle yaw input was increased by 2.3 degrees at 0.86 seconds, the 1R latitudinal point of rest would have been identically predicted. The yaw inputs used here were dictated by the published data and were not reanalyzed.

Given the sensitivity of the latitudinal result to yaw, we recommend the analyst examine any latitudinal deviation from the known occupant point of rest and calculate, given a predicted trajectory length, the angular yaw deviation that would have been required of the vehicle's attitude to match

the occupant's latitudinal point of rest exactly. Our validation analysis shows that despite our vehicle reconstruction yaw error of 2 to 3 degrees, occupant ejection results are still acceptable. However, in cases where the calculated yaw deviation becomes large, then either the vehicle's yaw input must be reconsidered, or the predicted mathematical solution is not a viable occupant trajectory.

We had hoped to compare ATD experimental landing times with the predicted landing times, as an additional model performance metric, since Exponent's video captured occupant ejection times via onboard, high-speed cameras [3]. Unfortunately, the stationary (off-board) high-speed cameras of the experimental scene followed the path of the vehicle as it rolled over, while the three ATDs of interest to this study were ejected so far beyond the vehicle's roll path that the ATDs quickly went out of view of the high speed cameras. Therefore, experimental landing times were not available.

We had also desired to compare ATD experimental landing positions with the predicted landing positions. While the scaled accident reconstruction diagram in Luepke *et al.* [4] did document ATD experimental PORs, it did not document ATD experimental points of landing. Similarly, the scaled accident reconstruction diagram in Carter *et al.* [2], did not document ATD experimental points of landing.

Indeed, all other efforts to recover any published and publicly available data beyond the results published in Funk *et al.* [17] were unfruitful. Therefore, we limited our assessment of the model's performance to prediction of experimental POR data and results from Funk *et al.* [4], shown in [Table 3](#).

In our engineering practice, we have observed some analysts ignore yaw effects altogether and shoehorn the 2D approach into a quasi-3D simulation by examining the accident sequence roll-by-roll, and reorienting the vehicle to approximate the vehicle's yaw in a piecewise fashion. While we appreciate this approach for its inventiveness, we have found it easier to simply write more comprehensive equations of motion, and let the mathematics relieve us from manual reorientations of the vehicle during the simulation.

Furthermore, we feel compelled to emphasize the utility of including yaw and yaw rate. In our years of using the model developed in [1], we have been able to rigorously accommodate occupant ejections from vehicles where yaw dynamics are dominant. For example, a vehicle that sustains a side impact and subsequently yaws for a quarter revolution or more is modeled as easily as the roll-only case. Moreover, cases where the vehicle yaws and then subsequently rolls is modeled without any increased effort. Finally, when the occupant's point of rest does not follow the vehicle's roll path, the use of yaw effects are compulsory. We have shown that even small vehicle yaw deviations, over large longitudinal throw distances, can have non-trivial effects on the occupant's

latitudinal deviations from the vehicle's straight-line path downstream.

Notice that we have placed the origin at the point of rest of the vehicle, as opposed to the point of trip of the vehicle, as done in our previous case example [1]. We do this because the vehicle point of rest does not change, whereas, the point of trip may change as the accident reconstruction is refined. Moreover, the occupant point of rest is often described relative to the vehicle point of rest, memorialized in photographs and police surveys. Finally, the biomechanical analyst may be asked to compare various occupant trajectories arising from two different accident reconstruction scenarios, prepared by two different parties. While the trip point may differ from reconstruction to reconstruction, the point-of-rest should be the same. Thus, the vehicle point of rest makes for a convenient datum. The transformation between a point of trip reference system and a point of rest reference system is simply an offset in the easting and northing directions.

A significant novelty of our work was to use the experimentally obtained instrumentation data from the dolly rollover with our model, and judge the results. An undertaking with instrumented data as a model input has not been previously published, and thus provided us with the opportunity for model validation. Although the dolly rollover test does not showcase yaw to the same degree that many real world accidents exhibit, we are convinced there is currently no better data that is published and publicly available. This work represents further confidence in the use of the previously developed model.

## **CONCLUSION**

We have applied experimental data from the dolly rollover test of the 1998 Ford Expedition to our mathematical model for occupant ejection to validate the model's ability to predict occupant trajectories. The model included a four degree-of-freedom description of vehicle motion: northing and easting translations, yaw and roll. Elevation changes and pitch degrees of freedom were assumed constant for all time. The model allowed for three degrees of freedom for motion of occupant motion: northing, easting, and elevation. The predicted occupant trajectory positions from ejection to rest matched actual data well.

## **REFERENCES**

1. Hovey, C.B., Kaplan, M.L., Piziali, R.L., "Occupant Trajectory Model using Case-Specific Accident Reconstruction Data for Vehicle Position, Roll, and Yaw," *SAE Int. J. Passeng. Cars - Mech. Syst.* 1(1):396-405, 2009, doi: [10.4271/2008-01-0517](https://doi.org/10.4271/2008-01-0517).
2. Carter, J.W., Luepke, P., Henry, K.C., Germane, G.J., Smith, J.W., "Rollover Dynamics: An Exploration of the

- Fundamentals," *SAE Int. J. Passeng. Cars - Mech. Syst.* 1(1): 80-104, 2009, doi: [10.4271/2008-01-0172](https://doi.org/10.4271/2008-01-0172).
3. Exponent, Failure Analysis Associates, Test and Engineering Center, Dolly Rollover Test, 1998 Ford Expedition, TEC9825, October 19, 2005.
  4. Luepke, P., Carhart, M., Croteau, J., Morrison, R., Loibl, J., Ridenour, J., "An Evaluation of Laminated Side Window Glass Performance During Rollover," SAE Technical Paper [2007-01-0367](https://doi.org/10.4271/2007-01-0367), 2007, doi: [10.4271/2007-01-0367](https://doi.org/10.4271/2007-01-0367).
  5. Anderson, J.D., Gee, R.S., Germane, G.J., Henry, K.C., DiBiase, S., Hoover, T., "Analysis of a Real-World High-Speed Crash from a Video Record and Physical Evidence," SAE Technical Paper [2008-01-1486](https://doi.org/10.4271/2008-01-1486), 2008, doi: [10.4271/2008-01-1486](https://doi.org/10.4271/2008-01-1486).
  6. Carter, J.W., Habberstad, J.L., Croteau, J., "A Comparison of the Controlled Rollover Impact System (CRIS) with the J2114 Dolly Rollover," SAE Technical Paper [2002-01-0694](https://doi.org/10.4271/2002-01-0694), 2002, doi: [10.4271/2002-01-0694](https://doi.org/10.4271/2002-01-0694).
  7. Cooperrider, N.K., Hammoud, S.A., Colwell, J., "Characteristics of Soil-Tripped Rollovers," SAE Technical Paper [980022](https://doi.org/10.4271/980022), 1998, doi: [10.4271/980022](https://doi.org/10.4271/980022).
  8. Funk, J.R., Wirth, J., Bonugli, E., Watson, R., Asay, A., "An Integrated Model of Rolling and Sliding in Rollover Crashes," SAE Technical Paper [2012-01-0605](https://doi.org/10.4271/2012-01-0605), 2012, doi: [10.4271/2012-01-0605](https://doi.org/10.4271/2012-01-0605).
  9. Rose, N.A., Beauchamp, G., "Development of a Variable Deceleration Rate Approach to Rollover Crash Reconstruction," *SAE Int. J. Passeng. Cars - Mech. Syst.* 2(1):308-332, 2009, doi: [10.4271/2009-01-0093](https://doi.org/10.4271/2009-01-0093).
  10. Thomas, T.M., Cooperrider, N.K., Hammoud, S.A., Woley, P.F., "Real World Rollovers - A Crash Test Procedure and Vehicle Kinematics," *Proc 12th International Conference on the Enhanced Safety of Vehicles*, pp. 819-825, 1989.
  11. Orlowski, K.F., Bundorf, R.T., Moffatt, E.A., "Rollover Crash Tests - The Influence of Roof Strength on Injury Mechanics," *Proc 29th Stapp Car Crash Conference*, paper 851734, 1985, doi: [10.4271/851734](https://doi.org/10.4271/851734).
  12. Parenteau, C., Gopal, M., Viano, D., "Near and Far-Side Adult Front Passenger Kinematics in a Vehicle Rollover," SAE Technical Paper [2001-01-0176](https://doi.org/10.4271/2001-01-0176), 2001, doi: [10.4271/2001-01-0176](https://doi.org/10.4271/2001-01-0176).
  13. Aronberg, R., "Airborne Trajectory Analysis Derivation for Use in Accident Reconstruction," SAE Technical Paper [900367](https://doi.org/10.4271/900367), 1990, doi: [10.4271/900367](https://doi.org/10.4271/900367).
  14. Searle, J.A., Searle, A., "The Trajectories of Pedestrians, Motorcycles, Motorcyclists, etc., Following a Road Accident," SAE Technical Paper [831622](https://doi.org/10.4271/831622), 1983, doi: [10.4271/831622](https://doi.org/10.4271/831622).
  15. Searle, J.A., "The Physics of Throw Distance in Accident Reconstruction," SAE Technical Paper [930659](https://doi.org/10.4271/930659), 1993, doi: [10.4271/930659](https://doi.org/10.4271/930659).
  16. Wood, D.P., "Application of a Pedestrian Impact Model to the Determination of Impact Speed," SAE Technical Paper [910814](https://doi.org/10.4271/910814), 1991, doi: [10.4271/910814](https://doi.org/10.4271/910814).
  17. Funk, J.R., Luepke, P.A., "Trajectory Model of Occupants Ejected in Rollover Crashes," SAE Technical Paper [2007-01-0742](https://doi.org/10.4271/2007-01-0742), 2007, doi: [10.4271/2007-01-0742](https://doi.org/10.4271/2007-01-0742).
  18. Herrera, J.M., Najera, A., Model for Analyzing Single Vehicle Rollover Accidents, Collision, The International Compendium for Crash Research, Vol 5, No 2, pp10-19, 2010.
  19. McCarron, E.S., Predicting Ejected Occupant Trajectories During Rollover, Proceedings of the 20th Canadian Multidisciplinary Road Safety Conference, Niagara Falls, Ontario, Jun 6-9, 2010.
  20. Funk, J.R., Beauchamp, G., Rose, N.A., Fenton, S.J., Pierce, J., "Occupant Ejection Trajectories in Rollover Crashes: Full-Scale Testing and Real World Cases," *SAE Int. J. Passeng. Cars - Mech. Syst.* 1(1):43-54, 2009, doi: [10.4271/2008-01-0166](https://doi.org/10.4271/2008-01-0166).
  21. Wood, D., Simms, C., "Coefficient of Friction in Pedestrian Throw," *Impact - Journal of Institute of Traffic Accident Investigators (ITAI)*, 9(1):12-15, 2000.
  22. Meyer, S.E., Herbst, B., Forrest, S., Syson, S.R., Sances, A., Kumaresan, S., "Restraints and Occupant Kinematics in Vehicular Rollovers," *Biomed Sci Instrum*, Vol 38, 465-469, 2002.
  23. Moffatt, E.A., James, M.B., "Headroom, Roof Crush, and Belted Excursion in Rollovers," SAE Technical Paper [2005-01-0942](https://doi.org/10.4271/2005-01-0942), 2005, doi: [10.4271/2005-01-0942](https://doi.org/10.4271/2005-01-0942).
  24. Moffat, E.A., Cooper, E.R., Croteau, J.J., Parenteau, C., Toglia, A., "Head Excursion of Seat Belted Cadaver, Volunteers and Hybrid III ATD in a Dynamic/Static Rollover Fixture," SAE Technical Paper [973347](https://doi.org/10.4271/973347), 1997, doi: [10.4271/973347](https://doi.org/10.4271/973347).
  25. Padmanaban, J., Moffatt, E.A., Marth, D.R., "Factors Influencing the Likelihood of Fatality and Serious/Fatal Injury in Single-Vehicle Rollover Crashes," SAE Technical Paper [2005-01-0944](https://doi.org/10.4271/2005-01-0944), 2005, doi: [10.4271/2005-01-0944](https://doi.org/10.4271/2005-01-0944).

## CONTACT

Chad B. Hovey, Ph.D.  
 Hovey Consulting LLC  
 4801 Lang Avenue NE, Suite 110  
 Albuquerque NM 87109  
 Telephone: 505-345-2070  
[chad.hovey@hoveyconsulting.com](mailto:chad.hovey@hoveyconsulting.com)

## APPENDIX

### APPENDIX A

Considering each of the terms from Eq. (4) successively, we have

$$\mathcal{F}\mathbf{v}^V = \begin{Bmatrix} \dot{x} \\ \dot{y} \\ \dot{z} \end{Bmatrix}, \quad (6)$$

which is simply the translational speed of the vehicle. The velocity  $\mathcal{V}\mathbf{v}^O$  in the inertial reference frame is given by  $\mathcal{F}\tilde{\mathbf{v}}^O = \mathcal{F}\mathbf{Q}^V \cdot \mathcal{V}\mathbf{v}^O$ , or explicitly by (7)

$$\mathcal{F}\tilde{\mathbf{v}}^O = \begin{Bmatrix} \dot{\chi} \cos \psi - \dot{\rho} \sin \psi (\cos \theta \cos \phi - \sin \theta \sin \phi) \\ \dot{\chi} \sin \psi + \dot{\rho} \cos \psi (\cos \theta \cos \phi - \sin \theta \sin \phi) \\ \dot{\rho} (\sin \theta \cos \phi + \cos \theta \sin \phi) \end{Bmatrix}, \quad (7)$$

where

$$\dot{\chi} = \mathcal{V}\mathbf{v}^O \cdot \hat{\mathbf{b}}_1, \quad (8)$$

where

$$\dot{\rho} = \sqrt{(\mathcal{V}\mathbf{v}^O \cdot \hat{\mathbf{b}}_2)^2 + (\mathcal{V}\mathbf{v}^O \cdot \hat{\mathbf{b}}_3)^2}, \quad (9)$$

and where the transformation matrix from the vehicle to inertial reference frame,  $\mathcal{F}\mathbf{Q}^V = \mathcal{F}\mathbf{Q}^C \cdot \mathcal{C}\mathbf{Q}^V$ , has been used, viz.,

$$\mathcal{F}\mathbf{Q}^V = \begin{bmatrix} \cos \psi & -\sin \psi \cos \theta & \sin \psi \sin \theta \\ \sin \psi & \cos \psi \cos \theta & -\cos \psi \sin \theta \\ 0 & \sin \theta & \cos \theta \end{bmatrix}. \quad (10)$$

The value  $\dot{\chi}$  is the speed of the occupant in the frame of the vehicle in the longitudinal direction of the vehicle (moving toward either the front or the rear of the vehicle). The value  $\dot{\rho}$  is the speed of the occupant in the frame of the vehicle in the radial direction, coplanar with the vehicle's roll plane spanned by  $[\hat{\mathbf{b}}_2, \hat{\mathbf{b}}_3]$ .

The final term in Eq. (4), expressed in  $\mathcal{F}$ , is given by

$$\mathcal{F}\boldsymbol{\omega}^V \times \mathbf{r}^{VO} = \begin{Bmatrix} \sin \psi \dot{\theta} \xi_3 - \dot{\psi} \xi_2 \\ -\cos \psi \dot{\theta} \xi_3 + \dot{\psi} \xi_1 \\ \cos \psi \dot{\theta} \xi_2 - \sin \psi \dot{\theta} \xi_1 \end{Bmatrix}, \quad (11)$$

where the explicit form for  $\mathbf{r}^{VO}$  expressed in the reference from  $\mathcal{F}$  is given by  $\mathcal{F}\mathbf{r}^{VO} = \{\xi_1, \xi_2, \xi_3\}^T$ , or

$$\begin{Bmatrix} \xi_1 \\ \xi_2 \\ \xi_3 \end{Bmatrix} = \begin{Bmatrix} \chi \cos \psi - \rho \sin \psi (\cos \theta \cos \phi - \sin \theta \sin \phi) \\ \chi \sin \psi + \rho \cos \psi (\cos \theta \cos \phi - \sin \theta \sin \phi) \\ \rho (\sin \theta \cos \phi + \cos \theta \sin \phi) \end{Bmatrix} \quad (12)$$

with

$$\chi = \mathcal{V}\mathbf{r}^{VO} \cdot \hat{\mathbf{b}}_1, \quad (13)$$

$$\rho = \sqrt{(\mathcal{V}\mathbf{r}^{VO} \cdot \hat{\mathbf{b}}_2)^2 + (\mathcal{V}\mathbf{r}^{VO} \cdot \hat{\mathbf{b}}_3)^2}, \quad (14)$$

and where the angular velocity vector is  $\mathcal{F}\boldsymbol{\omega}^V = \mathcal{F}\boldsymbol{\omega}^C + \mathcal{C}\boldsymbol{\omega}^V$ , or explicitly,

$$\mathcal{F}\boldsymbol{\omega}^V = \left\{ \begin{array}{c} \cos \psi \dot{\theta} \\ \sin \psi \dot{\theta} \\ \dot{\psi} \end{array} \right\}. \quad (15)$$

The Engineering Meetings Board has approved this paper for publication. It has successfully completed SAE's peer review process under the supervision of the session organizer. This process requires a minimum of three (3) reviews by industry experts.

All rights reserved. No part of this publication may be reproduced, stored in a retrieval system, or transmitted, in any form or by any means, electronic, mechanical, photocopying, recording, or otherwise, without the prior written permission of SAE.

ISSN 0148-7191

Positions and opinions advanced in this paper are those of the author(s) and not necessarily those of SAE. The author is solely responsible for the content of the paper.

**SAE Customer Service:**

Tel: 877-606-7323 (inside USA and Canada)

Tel: 724-776-4970 (outside USA)

Fax: 724-776-0790

Email: [CustomerService@sae.org](mailto:CustomerService@sae.org)

**SAE Web Address:** <http://www.sae.org>

**Printed in USA**

